International Journal of Thermal Sciences 48 (2009) 401–411

Contents lists available at ScienceDirect

International Journal of Thermal Sciences

www.elsevier.com/locate/ijts

An experimental study of a confined and submerged impinging jet heat transfer using Al_2O_3-water nanofluid

Cong Tam Nguyen [a,*], Nicolas Galanis [b], Guillaume Polidori [c], Stéphane Fohanno [c], Catalin V. Popa [c], Arnaud Le Bechec [d]

[a] Faculty of Engineering, Université de Moncton, Moncton, NB, Canada E1A 3E9
[b] Faculty of Engineering, Université de Sherbrooke, Québec, Canada J1K 2R1
[c] Faculté des Sciences, Universié de Reims, 51100, Reims, France
[d] Université de Bretagne Sud, I.U.P. de Lorient, 56321 Lorient, France

ARTICLE INFO

Article history:
Received 14 March 2008
Received in revised form 16 October 2008
Accepted 17 October 2008
Available online 8 November 2008

Keywords:
Impinging jet
Confined jet
Submerged jet
Forced convection
Heat transfer augmentation
Heat transfer enhancement
Nanofluid
Alumina–water nanofluid
Experimental study

ABSTRACT

An experimental investigation was performed to study the heat transfer performance of a 36 nm-Al_2O_3-particle–water nanofluid in a confined and submerged impinging jet on a flat, horizontal and circular heated surface. The tests were realized for the following ranges of the governing parameters: the nozzle diameter is 3 mm and the distance nozzle-to-heated-surface was set to 2, 5 and 10 mm; the flow Reynolds number varies from 3800 to 88 000, the Prandtl number from 5 to 10, and the particle volume fraction is ranging from 0 to 6%. Experimental data, obtained for both laminar and turbulent flow regimes, have clearly shown that, depending upon the combination of nozzle-to-heated surface distance and particle volume fraction, the use of a nanofluid can provide a heat transfer enhancement in some cases; conversely, for other combinations, an adverse effect on the convective heat transfer coefficient may occur. Within the experimental parameters used, it has been observed that highest surface heat transfer coefficients can be achieved using an intermediate nozzle-to-surface distance of 5 mm and a 2.8% particle volume fraction nanofluid. Nanofluids with high particle volume fractions, say 6% or higher, have been found not appropriate for the heat transfer enhancement purpose under the confined impinging jet configuration. On the other hand, for a very small and a large distance of nozzle-to-heated-surface, it has been observed that the nanofluid use does not provide a perceptible heat transfer enhancement and has, for some particular cases, produced a clear decrease of the convective heat transfer coefficient while compared to that obtained using distilled water.

1. Introduction

With a substantial increase of the power of the actual high performance microprocessors and various electronic components, considerable research efforts were deployed in the past few years in order to improve the heat transfer capabilities of those components. In spite of these efforts, cooling of high power electronic components still constitutes a rather challenging task (see in particular Leslie [1] and Nakayama [2]). In recent years, breakthroughs in manufacturing processes have permitted the creation of solid particles down to the nanometre scale, which in turn has resulted in the birth of a new and rather special class of fluids, named 'nanofluids', Choi [3]. These fluids seem to constitute a very interesting alternative for electronic cooling applications, Lee and Choi [4]. The term 'nanofluid' usually refers to a mixture composed of a saturated liquid where extremely fine nanoparticles are in suspension. To date, many nanoparticles dispersions of engineering interest are readily available from different commercial sources (see, for example, Nanophase Technologies [5]).

From a relatively limited amount of experimental data (see in particular Masuda et al. [6], Wang et al. [7], Chon et al. [8], Choi et al. [9], Eastman et al. [10], Roy et al. [11] and Angue Mintsa et al. [12]), it has been found that nanofluids generally possess thermal conductivities well higher than those of the base fluids. Some scarce experimental works (Pak and Cho [13] and Li and Xuan [14]) and numerical results (Maïga et al. [15] and Roy et al. [16]) have clearly assessed the heat transfer enhancement capability of these nanofluids in two particular confined flow situations, namely the flow inside a uniformly heated tube and the radial flow between heated disks. Such an advantageous effect of using nanofluids instead of conventional fluids for cooling of high heat output microprocessors has also been investigated both numerically and experimentally as well; see for example, Maré et al. [17] and Nguyen et al. [18,19]. It is worth noting that a use of nanofluids has its own drawbacks. In fact, it has been experimen-

* Corresponding author. Fax: +1 506 858 4082.
E-mail address: cong.tam.nguyen@umoncton.ca (C.T. Nguyen).

1290-0729/$ – see front matter
doi:10.1016/j.ijthermalsci.2008.10.007

Nomenclature

A	area of the heated exposed surface	m^2
C_p	fluid specific heat	J/kg K
d_i	diameter of the orifice	m
h	surface heat transfer coefficient	$W/m^2 K$
k	fluid thermal conductivity	W/m K
$\boldsymbol{m}$	mass flow rate	kg/s
Nu	Nusselt number, Eq. (5)	
q_{electric}	electric power input	W
Re	flow Reynolds number, Eq. (4)	
$T_{f,i}$	fluid inlet temperature	K or °C
$T_{f,m}$	fluid average temperature	K or °C
$T_{f,o}$	fluid outlet temperature	K or °C
T_S	surface temperature	K or °C

Greek symbols

μ	fluid dynamic viscosity	kg/m s
ρ	fluid density	kg/m^3
ϕ	particle volume fraction	

Subscripts

bf	refers to the base fluid
nf	refers to the nanofluid
p	refers to nanoparticles

tally found that with the presence of the nanoparticles within the base fluids, the dynamic viscosity of the resulting mixtures clearly increases drastically compared to that of the base fluids, see, for example, Masuda et al. [6] and Nguyen et al. [20]. Furthermore, it has also been observed that under the heating effect, the so-called 'hysteresis phenomenon' may occur on nanofluid viscosity (Nguyen et al. [20]). Finally, it should be mentioned (Keblinski et al. [21]) that there is a clear lack of data regarding the nanofluids behavior in real thermal applications and some other important issues; for example, the long term effects due to the temperature on the stability and suspension of these special mixtures remain unknown.

With respect to the problem under study that is the heat transfer and fluid flow of an impinging jet, there are numerous works, both experimental and numerical, which consider such a problem, see in particular the most recent studies [22–26]. A partial review of relevant works and studies may be found in Lee et al. [27] and Katti and Prabhu [28]. In these studies, both analytical/numerical and experimental, different jet configurations such as planar jet and slot jet, and various conditions such as confined jet and free jet, have been investigated. The following brief but exhaustive review is focused on some pertinent and relevant works close to the configuration under study. In particular, Baonga et al. [22] have measured local temperature and velocities profiles within a free liquid jet impinging on a circular horizontal heated disk using a laser induced fluorescence technique and image processing. They have also established the radial distribution the local heat transfer coefficient by solving the inverse heat conduction problem. Their data and results obtained for the average Nusselt number show that the influence of the nozzle-to-heat exchange surface spacing is light, and the Nusselt number clearly increases with nozzle diameter for the same Reynolds number. They also found that the evolution of the local heat transfer coefficient depends on the liquid flow rate. Xu and Galada [23] have developed an iterative and sequential inverse heat transfer analysis and, by implementing it into a two-dimensional finite element program, have thoroughly studied the heat transfer of water impinging jets in an industry scale test facility. Their results have shown that the heat transfer behavior at the stagnation point is mainly affected by the water temperature and hardly affected by water flow rate with mild effect from steel grade. Lin et al. [24] have experimentally investigated both the transient and steady-state cooling performance of a horizontal heat sink with a confined slot jet impingement. From their results obtained for both forced and mixed convection regimes show that effects of all the influencing parameters on the distribution of the normalized Nusselt number are not significant; two empirical correlations were proposed for computing the Nusselt number. Li et al. [25] numerically studied a 2-D laminar confined impinging slot jet and observed the existence of two different flow patterns, which depend on the flow Reynolds number, initial conditions, and geometry. Such dual solutions, verified by flow visualization, have been found to significantly affect the heat transfer. On the other hand, the flow and heat transfer in two planar impinging jets were investigated using Large-Eddy simulation and experiments by Akiyama et al. [26]. Their results and data have shown that forced jet results in significant changes to the flow structure with a rapid development of large-scale vortices in the shear layers emerging from the nozzle, which does not occur in an unforced jet. Also, the influence of the forcing raises the local Nusselt number in the vicinity of the stagnation line by about 10% compared to that of the unforced case. In their recent numerical study on a 2-D unsteady and confined impinging slot jet, Lee et al. [27] have found that the critical Reynolds number, beyond which the flow and thermal fields change their state from steady to unsteady, depends on the flow Reynolds number and height ratio. Also, the unsteadiness gives tremendous impact on the flow and temperature fields; different characteristics were found in the unsteady region compared to those of the steady region. Most recently, Katti and Prabhu [28] have experimentally investigated the effect of jet-to-plate spacing and Reynolds number on the local heat transfer distribution in an impinging submerged circular air jet on a smooth and flat plate. Three regions on the impinging surface were identified based on the flow characteristics of impinging jet, namely stagnation, transition and wall jet region, where local heat transfer coefficients are determined. It has been found that increase in Reynolds number increases the heat transfer at all the radial location for a given axial position. The existence of the second peak of local Nusselt number was found, which is believed to be due to the laminar-turbulent transition of the flow. Several semi-empirical correlations for local heat transfer rates have been proposed. There exists, to our knowledge, no available experimental data regarding the heat transfer performance of nanofluids under the geometrical configuration of a confined and submerged impinging jet.

In the present paper, we have experimentally investigated the heat transfer behavior of a confined impinging jet in a typical liquid cooling system, by replacing the base fluid (distilled water) by a nanofluid that is composed of distilled water and 36 nm-average-diameter-Al_2O_3 nanoparticles. Three particular nozzle-to-heated surface distances and two particle volume fractions were considered. Some significant results, experimental data, and observations are presented and discussed with emphasis on the heat transfer behavior of nanofluids.

2. Description of the experimental impinging jet system

The experimental liquid impinging jet system is relatively simple and consists of a closed fluid circuit, Fig. 1, which is mainly composed of a 10 litre open reservoir and a high head and all-

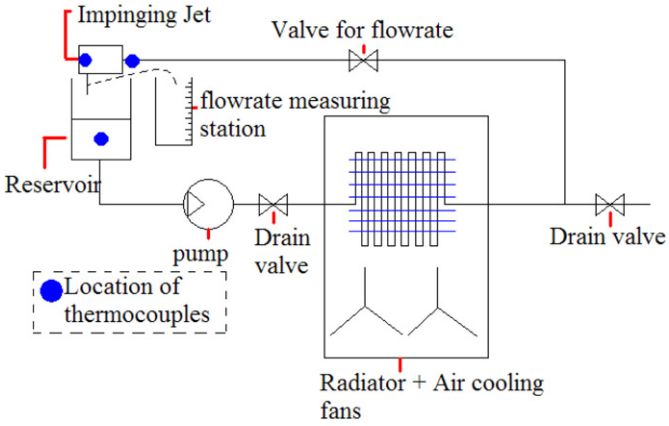

Fig. 1. Schematic illustration of the closed-fluid system used.

plastic magnetically-driven centrifugal pump that ensures a continuous forced circulation of liquid (distilled water or nanofluids). In order to create a horizontal circular heated surface, a heated block has been designed, Fig. 2a. This block, a cylindrical all-aluminum body of diameter 100 mm and overall length of 100 mm, is electrically heated by means of two standard 100 W nominal cartridge heaters (Omega, USA), which simulates heat generated by a high performance microprocessor or an electronic component. The top circular surface of this block, which is of diameter of 30 mm, is horizontal and mirror-machined. It constitutes the area on which is impinging the liquid jet that comes from a vertical nozzle (Fig. 2a). The nozzle diameter is 3 mm, and the vertical distance between that nozzle and the impacting heated horizontal surface can be set by using three precision mechanical guides. The nozzle-to-plate distance was carefully set and verified rigorously prior to and also after any test using prefabricated precision gauges. The whole body of the heated aluminum block is securely fixed on a thick and heavy wooden base. In order to minimize heat transmission from this block to its base as well as to other adjacent components, two thick Teflon disks are installed, one on the top around the 30 mm circular surface, and the other one in the bottom just between the aluminum block and its wooden base, Fig. 2a. The entire heated aluminum block unit is then thermally insulated with respect to the surrounding environment by using a 50 mm thick layer of Styrofoam wrapped all around the circumference of the unit, Fig. 2b. In order to create a confined space for the submerged jet, a Plexiglass cylindrical reservoir of diameter 125 mm and height of 150 mm has been installed on top of the upper Teflon disk, Figs. 2a and 2b. This reservoir, which is open to the atmosphere through a tiny orifice in its cylindrical cover, was always kept tightly closed in order to avoid any liquid splashing while operating the impinging jet system. On this reservoir wall, two separate outlet openings, located respectively at heights of 5 and 35 mm above the upper Teflon disk, offer two different thicknesses of the liquid layer above the circular heated surface. A mini air-cooled radiator is used to dissipate heat into the ambient air and a collecting-weighting station equipped with a three-way valve has been used for measuring the mass flow rate of the circulating liquid inside the system. It is worth noting that the above confined and submerged jet impinging system has especially been chosen in order to better represent the real system that exists in electronic cooling practices (see Leslie [1]).

Several Type-K thermocouples (Omega, USA) were installed at various locations in the liquid system in order to monitor fluid temperatures. The first one is placed in the fluid inlet pipe to measure the fluid temperature prior to the nozzle. The second one is placed in the 10 litre collecting reservoir to monitoring the fluid exit temperature. The third one, of the ceramic-insulator-type ther-

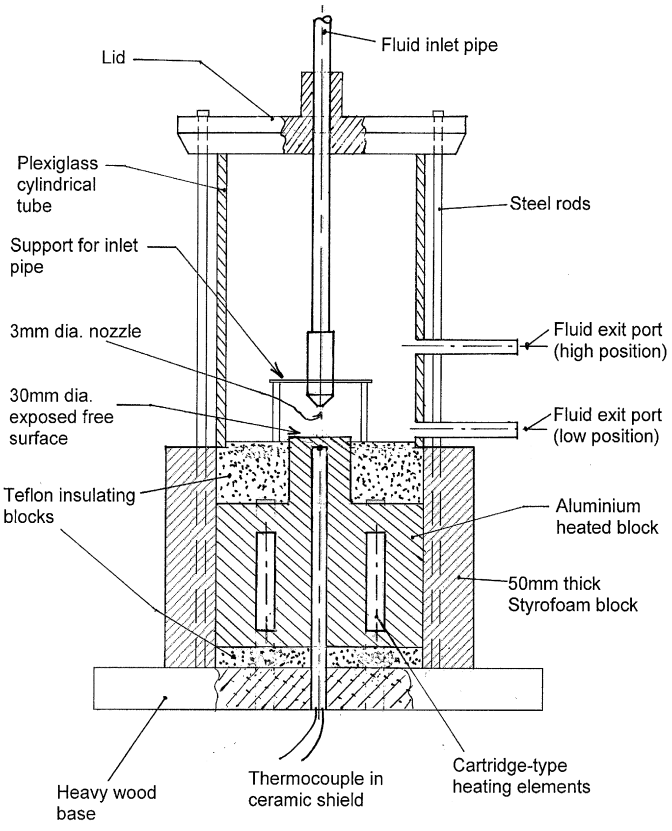

(a)

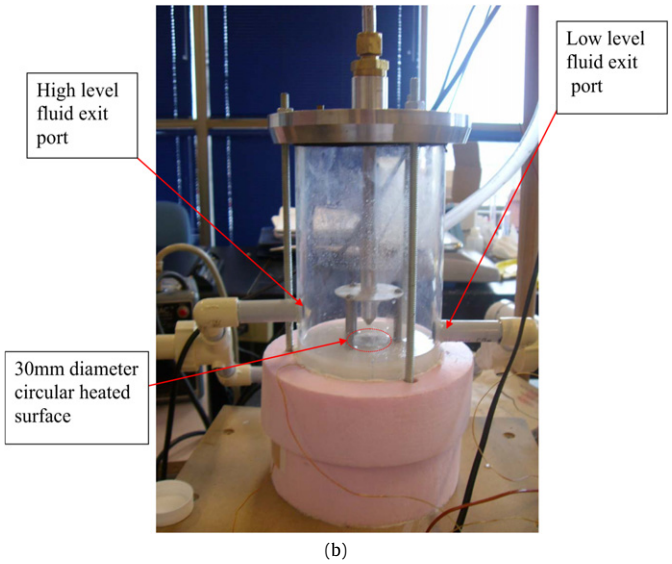

(b)

Fig. 2. (a) Schematic view of the confined impinging jet system used. (b) Photo showing the confined impinging jet system used.

mocouple, precisely mounted along the main axis inside a hole of the aluminum block, was especially chosen to measure the temperature within the solid region in the vicinity of the heated circular surface; its junction tip is located exactly at the distance 4.5 mm beneath the heated surface. In order to minimize the thermal contact resistance between the thermocouple tip and the block, a thin film of high thermal conductivity grease (Omegatherm 201 from Omega, USA) was applied at their contact interface. Another Type-K thermocouple has also been used to monitor the ambient air temperature in the laboratory. All thermocouples were thoroughly calibrated by using a constant temperature water bath, and

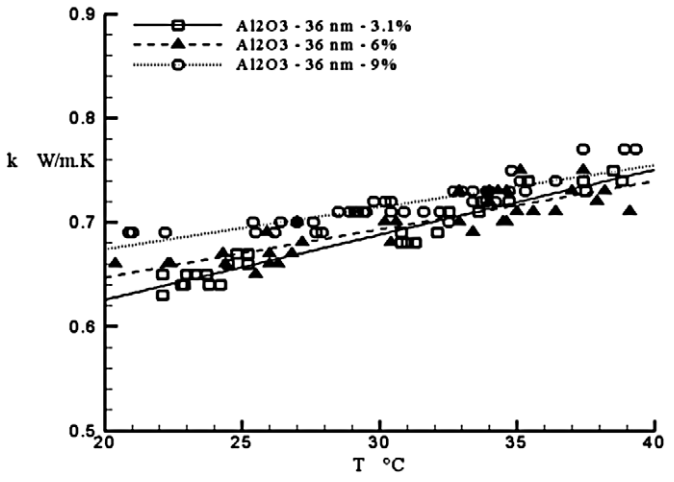

Fig. 3. Thermal conductivity data for 36 nm-Al_2O_3–water nanofluid.

their accuracy has been estimated to be ±0.2 K. A multi-channel digital indicator has been used to display all readings from the thermocouples.

In order to precisely calculate the total electric power that is supplied to the cartridge heaters and indirectly, the heat supplied to the aluminum heated block, both the AC voltage and electric current were constantly monitored during the tests. It has been found that the accuracy of the computed electric power can be estimated to be ±3.5%. With regard to the heat losses from the heated-block-and-base ensemble towards the ambient air, the temperature drop across the insulating Styrofoam layer as well as that through the bottom Teflon disk has been monitored during every experiment. And the corresponding total heat loss of the unit can then be easily estimated, which has been found to be negligible as it did not exceed, so far 1.5 W, i.e. approximately 1.5% of the total heat input. Finally, with regards to the measurement of the mass flow rate, we have adopted, in this study, the conventional stop-watch-and-weighting technique, by using high precision digital balance and chronometer; their accuracies are estimated, respectively, ±0.1 g and ±0.01 s. The maximum variation of the mass flow rate as determined by such a simple and reliable technique has been estimated to be ±5%, an error that appears quite reasonable when considering all of the other experimental uncertainties.

2.1. Thermo-physical properties of the Al_2O_3–water nanofluid used

For the nanofluid under study, namely water–Al_2O_3 (36 nm average particle diameter), by assuming that a constant and uniform particle volume fraction prevails throughout the fluid circuit, and knowing the constituent properties, the effective thermo-physical properties of this nanofluid can then be evaluated using classical formulas already derived and well known for a two-phase fluid (see in particular, Xuan and Roetzel [29]). In the following equations used for computing the nanofluid density and specific heat, the subscripts p, bf and nf refer, respectively, to the particle, the base fluid and the nanofluid; Φ is the particle volume fraction:

$$\rho_{nf} = (1-\phi)\rho_{bf} + \phi\rho_p \tag{1}$$

$$(\rho \cdot C_p)_{nf} = (1-\phi)(\rho \cdot C_p)_{bf} + \phi(\rho \cdot C_p)_p \tag{2}$$

For Al_2O_3-36 nm nanoparticles properties, the following data are used: density $\rho_p = 3600$ kg/m^3 and specific heat $(C_p)_p = 773$ J/kg K. In particular, regarding the thermal conductivity and dynamic viscosity, recent experimental data obtained by our research group—data that are specific to the nanofluid under study—are available. Figs. 3 and 4 show respectively the corresponding data employed for the nanofluid thermal conductivity and dynamic viscosity (the complete databases were detailed in Angue Mintsa et al. [12] and Nguyen et al. [20]). Finally, regarding the thermal properties of distilled water, they have been evaluated using classical formulas published in standard textbooks; see for example, Hagen [30].

2.2. Experimental procedures and data processing

The experimental liquid circuit, Fig. 1, was first thoroughly checked for possible leaks from various connexions. The system was then used to perform nearly forty tests using distilled water and Al_2O_3–water nanofluid for three different nozzle-heated-surface distances, namely 2, 5 and 10 mm. For each of these distances, three different particle volume fractions, namely 0% (i.e. distilled water), 2.8 and 6%, were considered. It is interesting to mention that the Al_2O_3–water nanofluid, with average particle diameter of 36 nm, was purchased readily prepared and mixed from a commercial source (Nanophase Technologies, USA). Such a mixture appears appropriate for use in thermal applications. At delivery, the original solution possesses a particle volume fraction of nearly 22%. In order to create several other solutions with particular particle fractions from such an original mixture, a proper diluting process with distilled water combined with a vigorous mechanical stirring action has been found sufficient to have a good particle dispersion and suspension. It is worth mentioning that since dispersant agents were used by the manufacturer, the stability of the particle suspension within distilled water seems to be quite acceptable (at least for particle volume fractions lower than 6%). It has been observed that even after a relatively long resting period, say several days to weeks, only a vigorous stirring action was normally sufficient to properly restore the particle suspension.

From the collected data for the fluid inlet temperature and mass flow rate, the average surface convective heat transfer coefficient under the impinging confined jet, h (W/m^2 K), can easily be deducted from the following heat balance equation:

$$q_{\text{electric}} = hA(T_s - T_{f,i}) = \boldsymbol{m} C_p (T_{f,o} - T_{f,i}) \tag{3}$$

where q_{electric} is the total electric input power, W; $\boldsymbol{m}$ is the mass flow rate, kg/s; $T_s, T_{f,i}$ and $T_{f,o}$ are, respectively, the average temperature of the heated surface, the inlet and outlet temperatures of the fluid, K or °C; A is the area of the heated circular surface, m^2; all fluid properties were evaluated at $T_{f,m}$ where $T_{f,m} = 0.5(T_{f,i} + T_{f,o})$. It should be noted that the surface temperature T_s was not measured, but estimated instead from the corresponding measured temperature of the solid at the precise distance of 4.5 mm beneath the heated surface. Since the heated aluminum block was thermally insulated so that ones can assume that the one-dimensional heat conduction prevails along the upward axial direction inside the small cylinder below the heated surface (see again Figs. 2a and 2b). Knowing the total heat input, the heated surface temperature is then easily computed. Finally, it is worth mentioning that in order to minimizing errors, the average surface heat transfer coefficient by Eq. (3) has been calculated using the values computed for q_{electric}. So far, the experimental uncertainty has been estimated to be ±5.5% for the values of the surface heat transfer coefficient.

For a general presentation of the results hereafter, the following definition is introduced for the flow Reynolds number and the average Nusselt number:

$$Re = 4\boldsymbol{m}/(\pi d_i \mu) \tag{4}$$

$$Nu = h d_i / k \tag{5}$$

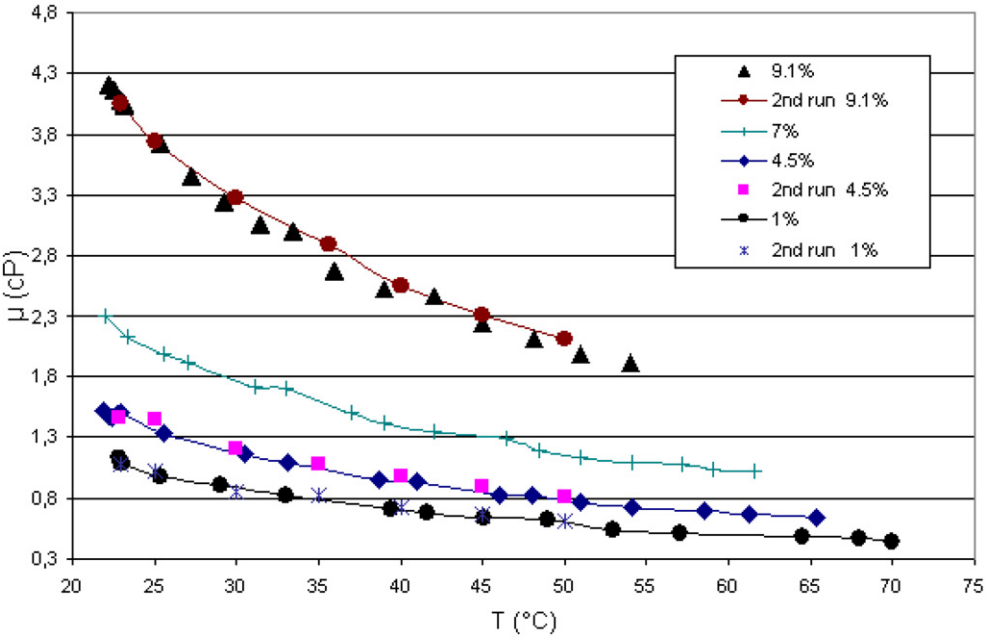

Fig. 4. Dynamic viscosity data for 36 nm-Al_2O_3–water nanofluid.

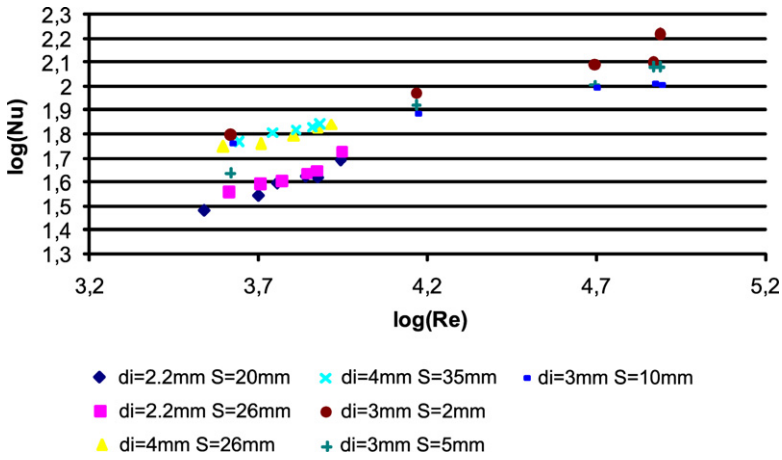

Fig. 5. Variation of Nu as function of Re for distilled water, comparison with Baonga et al.'s [22] experimental data.

where d_i is the inside diameter of the nozzle orifice, $d_i = 3$ mm; k and μ are fluid (distilled water or nanofluid) thermal conductivity and dynamic viscosity; all fluid properties are evaluated at the fluid mean temperature $T_{f,m}$. It is worth noting that a maximum uncertainty of $\pm 10.5\%$ can be expected for the computed values of the average Nusselt number.

Finally, it is worth noting that there must be a radial variation of the heated surface temperature and, consequently, of the surface heat transfer coefficient as well. In the present study, we have adopted an 'average' approach, in which the approximately 'averaged' heat transfer coefficient is deduced, using Eq. (3), and knowing the total electric power supplied and the estimated 'pseudo-averaged' surface temperature. This approach was motivated by two main reasons. First, as the heated surface is of a small dimension, only 30 mm in diameter, and made from a high thermal conductivity aluminum, and because of the unidirectional heat conduction inside the heated bloc, it is reasonable to believe that the solid temperature, at a given axial coordinate, would be nearly uniform along the radial direction, i.e. the radial gradient of temperature is less pronounced than that along the axial direction. Hence, the estimated surface temperature at the stagnation point would approximately represent the 'averaged' surface temperature. Secondly, due to the presence of the heating cartridges installed inside the aluminum bloc, it was rather difficult, although we would like to, to precisely measure local surface and fluid temperatures along the radial direction in order to assess any variation of the heat transfer. Such an 'average' approach could not give any information regarding the radial behavior of heat transfer. However, on a global basis, it is reasonable to believe that the data and results shown in this paper are physically realistic and give a genuine portrait of the nanofluid heat transfer behavior in a confined and submerged impingement jet system.

3. Results and discussion

3.1. Results obtained from tests using distilled water

Due to our specific geometry of the confined impinging jet considered, it was rather difficult to find out studies that consider a similar geometry to which a proper comparison can be performed. The only study that appears to be relatively close to the present study is the one by Baonga et al. [22]. Fig. 5 shows, in particular, the measured data as obtained for the average impinging jet Nusselt number for several tests performed using distilled water.

For comparison purposes, some corresponding data obtained by Baonga and colleagues, for 2.2 and 4 mm nozzle diameters, are also shown, where S indicates the nozzle-to-heated surface distance. Although all the results have shown a similar trend regarding the increase of the Nusselt number with respect to the flow Reynolds number, there is obviously a pronounced difference between the present data and the ones by Baonga and colleagues. In fact, the present data seem to be consistently higher than the latter. Such a difference may be explained by two folds. First, Baonga et al. [22] have considered the case of a free jet impinging on an open heated surface, while in the present study the impinging jet flow is confined because of the presence of the Plexiglass reservoir. As consequence, in contrast to the radial outward flow found in their study, we have observed a strong and swirling flow of water on the heated surface. Such a swirling effect is believed to be a key factor that has favorably contributed to the heat transfer enhancement found in our case. A second reason that may explain the occurrence of higher surface heat transfer coefficients in the present study resides in the fact that Baonga et al. [22] used considerably larger nozzle-to-heated-surface distances (which varied from 20 to 35 mm) while in our investigation, such a gap distance was ranging from 2 to 10 mm. Therefore, it is obvious that under a higher convection effect resulting from a higher fluid impacting velocity in the vicinity of the stagnation zone, a higher surface heat transfer rate can then be expected as found in Fig. 5. Finally, it is worth noting that Baonga et al.'s [22] data are concerned with relatively low mass flow rate, the flow Reynolds number remain less than 10 000, while in the present study, this parameter is ranging from 4000 to nearly 80 000 for tests using distilled water.

3.2. Effect of using nanofluid on the surface temperature under impinging jet

Fig. 6 (a, b, c) shows the results obtained for the temperature difference $\Delta T = T_s - T_{f,i}$ (then indirectly, the heated surface temperature) as a function of the mass flow rate and particle volume fractions; the nozzle-to-heated surface distance was set, respectively, to 2, 5 and 10 mm, and the total heat input was adjusted to 100 W approximately. One can clearly observe that, in general, the temperature difference ΔT has clearly decreased with an augmentation of the mass flow rate. Such behavior is obviously due to the fact that with increasing mass flow rate, the forced convection effect also increases considerably, which in turn, augments the heat transfer within the fluid in general. Thus, for a given fluid inlet temperature, the heated surface temperature would logically decrease for higher mass flow rate. Such a result has consistently been observed for water, the two nanofluids (2.8 and 6% of particle fractions) and three distances nozzle-to-heated surface tested. With regard to the nanofluid effects on ΔT relative to that of distilled water, the results shown have revealed that a use of nanofluids does not necessary provide a lower value of ΔT. Thus, for the case of a 2 mm distance for example, Fig. 6a, one can observe that, surprisingly, it is distilled water that provides, for a given mass flow rate, a lowest value. On the other hand, the 6% particle-volume-fraction nanofluid gives the highest values for ΔT. For the 5 mm distance, Fig. 6b, we can observe again that the 6% nanofluid gives the highest values for ΔT, while water and the 2.8% nanofluid provide approximately equivalent values for ΔT. A similar behavior can be noticed through Fig. 6c for the 10 mm distance. In other words, for the experimental test conditions, the nanofluid with 6% particle volume fraction seems not to be appropriate for use as a means for the heat transfer enhancement purpose.

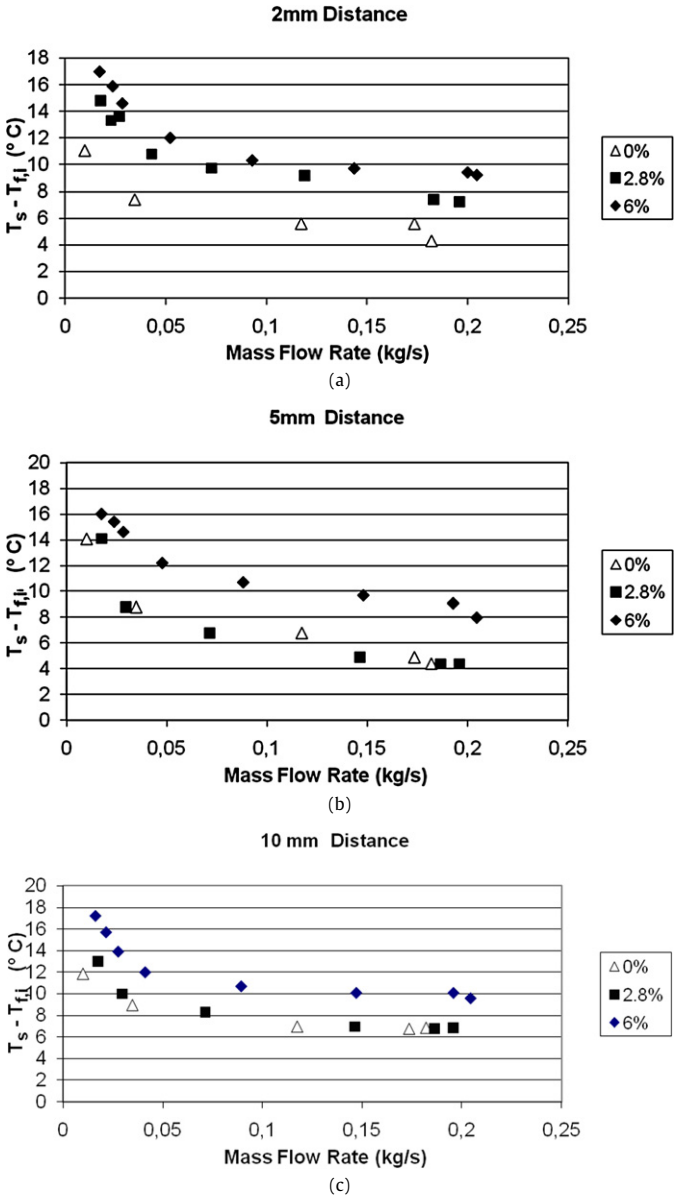

Fig. 6. (a) Variation of the heated surface temperature (2 mm distance). (b) Variation of the heated surface temperature (5 mm distance). (c) Variation of the heated surface temperature (10 mm distance).

3.3. Nanofluid heat transfer under a confined impinging jet

In order to better understand the heat transfer behavior of nanofluids under a confined impinging jet, the results obtained for the surface heat transfer coefficient (deduced by using Eq. (3)) are shown on Figs. 7a, 7b and 7c, respectively, for 2, 5 and 10 mm distances, and this as a function of the mass flow rate and particle volume fraction.

It is interesting to observe, at first, that the heat transfer coefficient on the heated surface increases considerably with an increase of the mass flow rate. Such behavior, observed for both water and the nanofluids considered, is obviously a direct consequence of an increasing convection effect under a higher mass flow rate. It is worth noting that, although a direct comparison was not possible because of difference in the geometry tested, such behavior appears quite consistent with Baonga et al.'s [22] data (see again Fig. 5). This behavior is also found qualitatively concordant while compared to that observed by Katti and Prabhu [28], although these authors only provided local heat transfer data. Secondly,

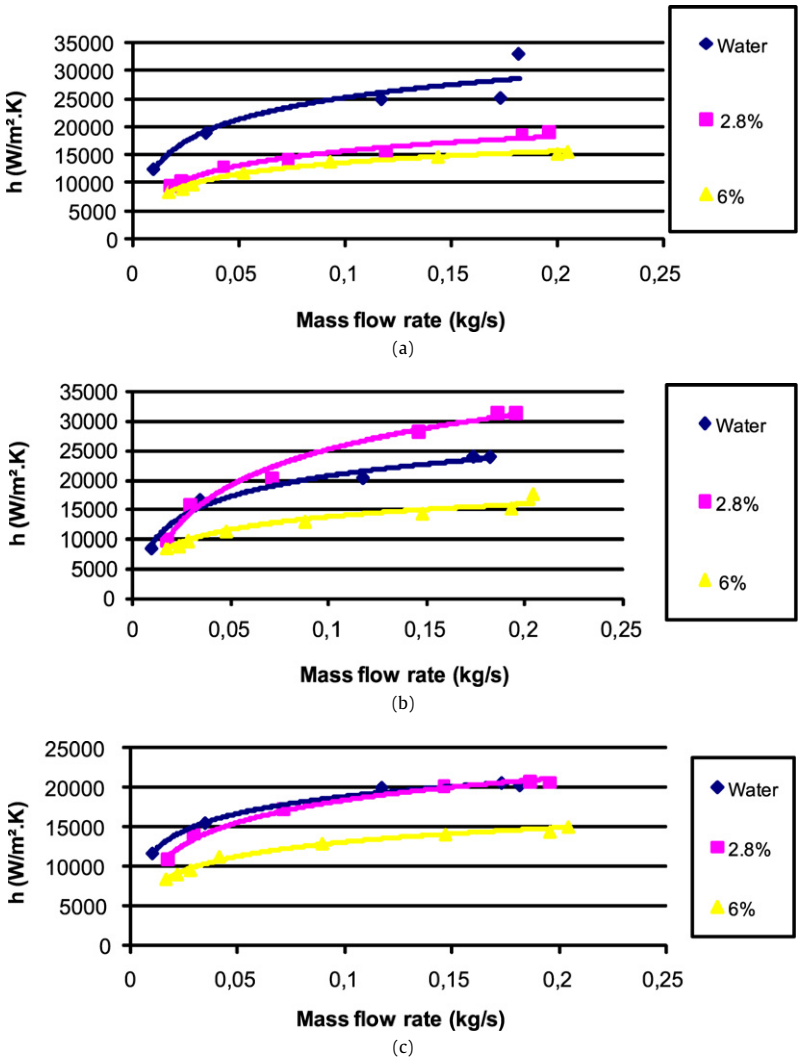

Fig. 7. (a) Variation of h function of mass flow rate and particle volume fraction (2 mm distance). (b) Variation of h function of mass flow rate and particle volume fraction (5 mm distance). (c) Variation of h function of mass flow rate and particle volume fraction (10 mm distance).

from the results shown, one may remark that the use of nanofluids does not always guaranty an enhancement of heat transfer under the confined impacting jet. In fact, it is apparent that depending upon the particular combination of the nozzle-to-heated-surface distance and the particle volume fraction, some heat transfer augmentation can be achieved. However, for other combinations, adverse results, i.e. a decrease of the surface heat transfer coefficient, have been found. Thus, for the cases with 2 mm distance in particular (Fig. 7a), distilled water is actually the one that gives, for a given mass flow rate, highest heat transfer coefficients; in contrast, for the two nanofluids tested, 2.8 and 6% of particle volume fractions, the heat transfer coefficients remain appreciably lower than those corresponding to water. Thus, for example, for the particular mass flow rate $\boldsymbol{m} = 0.15$ kg/s, the computed values for h are, respectively, 27 500 W/m^2 °C (water), 17 500 W/m^2 °C (2.8%) and 15 000 W/m^2 °C (6%), i.e. a drastic decrease of nearly 45% by using a 6% nanofluid while compared to water. A reverse trend was found, however, for the nozzle-to-heated-surface distance of 5 mm (Fig. 7b). In fact, it is very interesting to observe that the 2.8% nanofluid is now the one that clearly gives highest heat transfer coefficients, which is followed by water and, in the third place, by the 6% nanofluid. Again, for the mass flow rate of $\boldsymbol{m} = 0.15$ kg/s in particular, the convective heat transfer coefficient h has as values, 23 000 W/m^2 °C for water, 29 000 W/m^2 °C for 2.8% and 15 000 W/m^2 °C for 6%; thus, an increase of almost 26% by using a 2.8% particle volume fraction nanofluid over that provided by water. From the results obtained for 5 mm distance, one may expect that there exists an optimal particle volume fraction that would maximize the surface heat transfer. Such an interesting issue will be considered in our future research program. Finally, for the 10 mm gap distance (Fig. 7c), it is very interesting to observe that both distilled water and the 2.8% nanofluid have provided almost the same heat transfer performance: the two corresponding curves are, in fact, nearly superposed on one other, and give values for h that are clearly higher than the ones obtained by using the 6% nanofluid. For a mass flow rate $\boldsymbol{m} = 0.15$ kg/s, for example, the values of the surface heat transfer coefficient are, respectively, 20 000 W/m^2 °C for both water and 2.8% nanofluid, and only 14 000 W/m^2 °C for the 6% nanofluid. Thus, for this particular nozzle-to-heated-surface distance, it seems that the use of nanofluids does not provide a perceptible heat transfer enhancement. Finally, it is worth noting that in spite of the experimental uncertainties and except for only one case involving distilled water, all the data points, for a specific case, fall close to the corresponding fitted-curve. Such result clearly shows the trends regarding nanofluid heat transfer behavior.

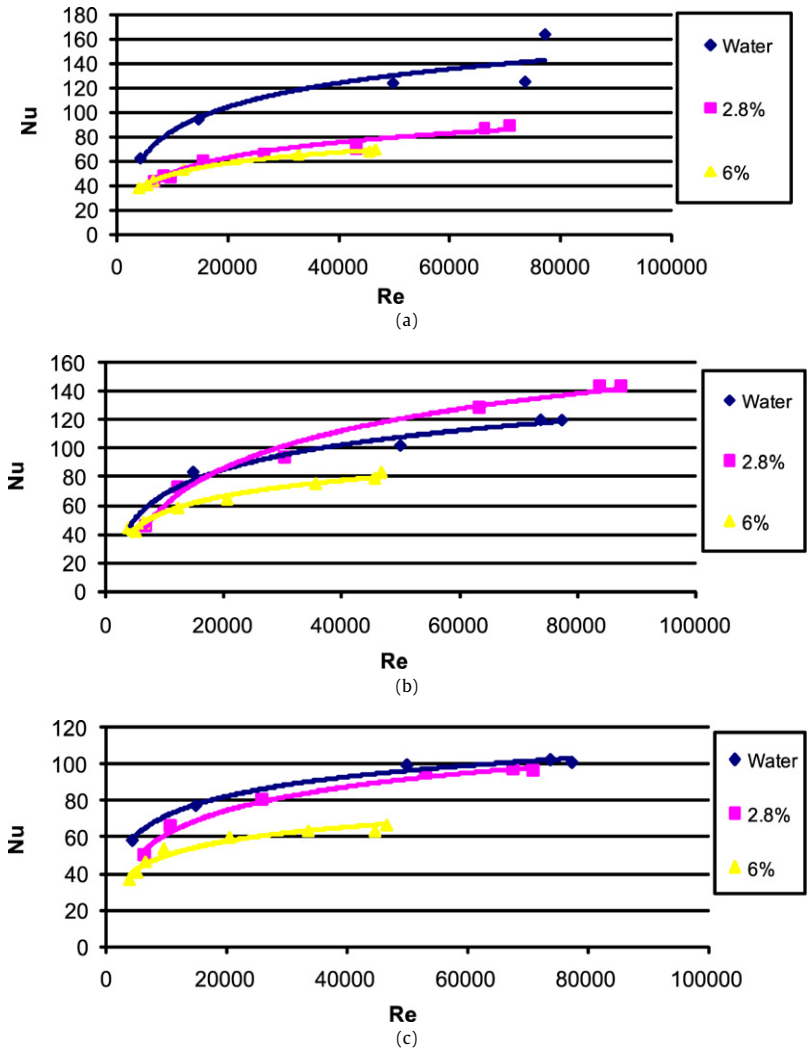

Fig. 8. (a) Variation of *Nu* function of *Re* and particle volume fraction (2 mm distance). (b) Variation of *Nu* function of *Re* and particle volume fraction (5 mm distance). (c) Variation of *Nu* function of *Re* and particle volume fraction (10 mm distance).

3.4. Variation of Nu as function of Re and particle volume fraction

Figs. 8a, 8b and 8c show, respectively, for 2, 5 and 10 mm distances, the corresponding results obtained for the heated surface average Nusselt number (Eq. (5)) as a function of the flow Reynolds number *Re* (Eq. (4)) and particle volume fraction (it is worth noting that the definition of the average Nusselt number includes variations not only of the surface convective heat transfer coefficient but of the nanofluid thermal conductivity as well). Here again, we can easily observe the same behavior regarding the dependence of *Nu* with respect to the parameter *Re* and particle volume fraction. Thus, within the range of the experimental parameters considered, the use of a nanofluid can conduct to an adverse effect on the heat transfer in the case of a very small nozzle-to-surface distance, say for 2 mm distance for example. For the latter, it is clear that using water would be better after all, Fig. 8a. Such a comment also holds for a large nozzle-to-surface distance, say for a 10 mm distance, for example, Fig. 8c. The heat transfer enhancement capability of a nanofluid is only observed for the case of an intermediate distance, 5 mm in particular (Fig. 8b), and this when combined with a relatively low particle volume fraction, 2.8%. Again, such a heat transfer enhancement appears to be more important for higher mass flow rates. Finally, for the 10 mm distance (Fig. 8c): very close values of *Nu* have been obtained by water and the 2.8% particle fraction nanofluid, while the 6% nanofluid offers mediocre performance. It is interesting to mention that, to our knowledge, the heat transfer data presented here regarding the use of a nanofluid under a confined impinging jet are believed to be the first of its kind. The authors hope that these data will contribute to an understanding of the nanofluid thermal behavior in practical application.

In order to create a more generalized presentation of heat transfer data, we have attempted to regroup them under the form of $\mathrm{Log}(Nu/Pr^{0.4})$ function of the flow parameter, $\mathrm{Log}(Re)$ and the particle volume fraction. Fig. 9 shows such a presentation, in which each set of results includes all data obtained for the three nozzle-to-surface distances studied. It is worth mentioning that for the data shown, the Prandtl number, which is evaluated at the fluid mean temperature $T_{f,m}$, varies from 5 to nearly 10. One can observe that, in spite of some visible dispersion due to experimental uncertainties and, of course, to a change of the heat transfer rate with respect to the nozzle-to-surface distance, data for a specific particle volume fraction seem to follow a certain pattern. The different straight lines obtained using a standard least-squares approximation technique show clearly the influence due to the particle volume fraction. One can expect that within the experimental parameter ranges tested, such a 'unified' presentation as shown on Fig. 9 may be useful for estimating the surface heat transfer in various practical thermal applications involving confined impinging jet using nanofluids.

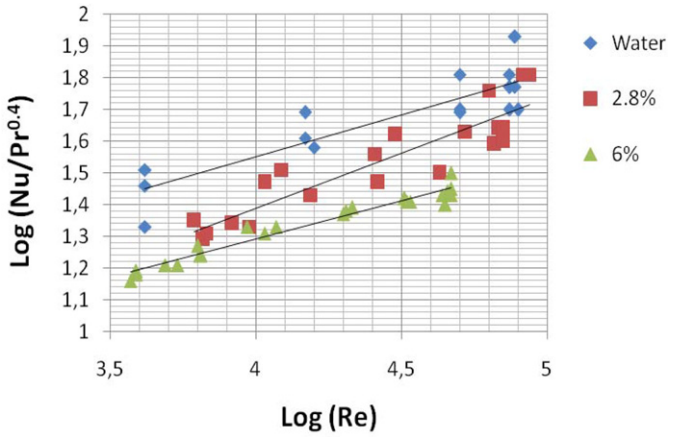

Fig. 9. Variation of Log($Nu/Pr^{0.4}$) function of Log(Re) and particle volume fraction for all nozzle-to-surface distances tested.

3.5. Effect of the nozzle-to-surface distance on nanofluid heat transfer coefficient

From the results shown in Figs. 7 (a, b and c) and 8 (a, b, and c), one can observe, at first, that for distilled water, increasing the distance from the nozzle to the heated surface has produced a considerable decrease of the convective heat transfer coefficient. Thus for $Re = 60\,000$, for example, the surface average Nusselt has as approximate values, 135, 112 and 100, respectively, for distances of 2, 5 and 10 mm. Such a decrease of the heat transfer coefficient can be explained by the fact that with a greater distance from the heated surface and for a given mass flow rate, the fluid velocity impacting on the heated surface, in the vicinity of the stagnation zone, would decrease. As consequence, the fluid radial and outward velocity within the boundary layer also decreases. Furthermore, as mentioned before, for the case of a confined impinging jet as the one under study here, there is a constant swirling flow due to the presence of a cylindrical shroud surrounding the jet orifice. It has been clearly observed during the experiments that this swirling flow, which exists for all tests and has, indeed, a favorable effect on the surface heat transfer, also decreases in intensity when the nozzle moves away from the heated surface. As a consequence, the surface heat transfer coefficient has been found to decrease appreciably with an increase of the distance between the jet nozzle and the surface.

The effect due to the nozzle-to-surface distance on the heat transfer appears quite different for the nanofluids considered. Thus for the 2.8% particle volume fraction nanofluid in particular, see again Figs. 8a, 8b and 8c, one can see that for $Re = 60\,000$, for example, the average Nusselt number increases from 82 (for 2 mm distance) to nearly 130 (for 5 mm) but decreases to 95 (for 10 mm). For this particular particle volume fraction, in light of the results obtained, one can expect that there may exist an optimal distance that gives the highest heat transfer coefficient. On the other hand, for the nanofluid with 6% particle volume fraction and for $Re = 40\,000$, for example, the parameter Nu has, as approximate values, 68, 78 and 65, respectively, for the distances of 2, 5 and 10 mm.

3.6. Some explanation regarding nanofluid heat transfer under a confined, submerged impinging jet

The above heat transfer results under the configuration of a confined impinging jet have revealed a somewhat surprising and intriguing behavior of the nanofluids used. In fact, as stated previously, for some particular combinations of nozzle-to-surface distance-and-particle volume fraction, an adverse effect, i.e. a decrease of the convective heat transfer coefficient may even occur. In particular, for a small nozzle-to-surface distance, say 2 mm, as well as for a larger one, say 10 mm, the use of the 36 nm-Al_2O_3–water nanofluid does not provide any heat transfer enhancement; only for an intermediate distance, say 5 mm, the use of a low particle volume fraction nanofluid, 2.8% in particular, has produced a considerable heat transfer increase, see again Figs. 7b and 8b. Also, a nanofluid with higher particle volume fraction, say 6% or more, should be avoided as it does produce worse heat transfer performance, according to our data.

Such behavior may appear unusual as it is contrary to the trend often observed when using nanofluids in thermal applications. In fact, based on some experimental data available in the literature, it has been found that for some confined flow situations, the use of nanofluids has provided a clear heat transfer enhancement (see in particular Lee and Choi [4], Pak and Cho [13], Li and Xuan [14] and Nguyen et al. [19]). In spite of the fact that there exists no general theoretical model available to date that can satisfactorily explain the heat transfer enhancement capability of nanofluids — see in particular Xuan and Roetzel [29] and Keblinski et al. [21] — it is believed that a heat transfer augmentation achieved by using nanofluids is mainly due to their improved thermal properties as well as to the thermal diffusion effect, diffusion that is induced within the base fluid by the Brownian movement of the nanoparticles themselves.

With regard to the present case of a submerged, confined impinging jet and nanofluids heat transfer data, due to the particularity of the geometry considered, we believe that the existence of a large recirculation fluid zone that is present on top of the radial outward flow (i.e. the one generated by the impacting fluid on the heated surface) has an important effect on the nanofluid heat transfer behavior. In fact, as it can be seen on Fig. 10 that shows an illustrative view of the internal flow structure inside the Plexiglass reservoir, such a recirculation zone creates a certain obstruction for the proper evacuation of the heated fluid itself (unfortunately, due to nanofluid high opacity, the capture of such a flow structure, although being observed during the course of experiences, was not possible). For the cases with a small nozzle-to-surface distance, 2 mm in particular, as the direct impacting jet affects only a small area of the heated surface, it is expected that this recirculation zone may be quite large and occupy a major portion of the liquid layer within the reservoir. Since hot nanofluid is 'entrapped' inside the recirculation zone, it creates an unfavorable effect when interacted with the radial outward flow of heated fluid located near the reservoir bottom surface. As consequence, the cooling of the heated surface can be reduced. Such an unfavorable effect may become more pronounced when using a nanofluid with higher particle volume fraction, because of the fact that a higher thermal conductivity would result in a higher temperature of the nanofluid parcel trapped inside the recirculation zone. This can explain a mediocre heat transfer performance found for the nanofluids tested, in particular for the one with 6% particle volume fraction (see again Figs. 7a and 8a). For the cases with 5 mm nozzle-to-surface distance (Figs. 7b and 8b), as the nozzle moves farther from the heated surface (in fact, the nozzle orifice is approximately at the free surface of the liquid layer), the direct impinging jet now affects a larger area of the heated surface. The above recirculation fluid zone diminishes both in thickness and in volume, thus allows a stronger radial outward flow along the heated surface that, in turn, results in a more pronounced convection effect. The heat transfer rate hence becomes more important, at least for the case of 2.8% nanofluid. For the case of the 6% nanofluid however, which is quite viscous (its dynamic viscosity is twice of that of water near ambient temperature), it is believed that the resulting fluid flow is much slower that, when combined with the unfavorable effect due to the recirculation zone discussed above, it causes a drastic decrease of the surface heat

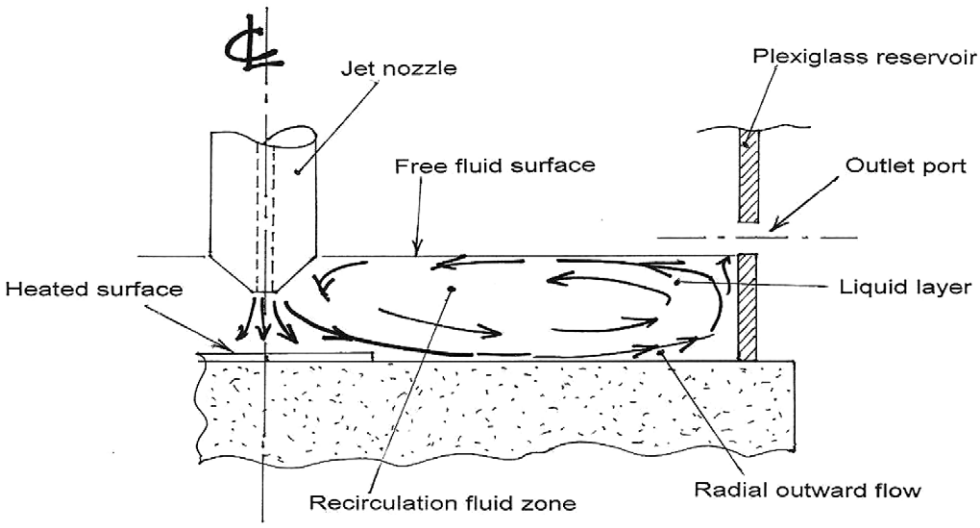

Fig. 10. An illustrative view of the internal flow structure inside the reservoir.

transfer rate, i.e. when compared to that of the 2.8% nanofluid and even to the one of water. Finally, for the case of a large nozzle-to-heated surface distance, 10 mm in particular, as the nozzle is now located above the free surface of the liquid layer (the thickness of such liquid layer is approximately 5 mm), one can expect that the impacting fluid velocity on the heated surface is considerably decreased compared to other cases, and hence the convective heat transfer is generally reduced. For the same reasons mentioned earlier, the highly viscous 6% nanofluid is again the one that offers the lowest convective heat transfer rates (Fig. 7c).

The above explanation, although physically plausible, may be not sufficient to fully explain a large difference observed on heat transfer coefficients as provided by distilled water and by nanofluids, in particular by the 6% nanofluid that exhibits a worse heat transfer performance. Under the condition of a highly turbulent shear flow as the one studied here, it is plausible to expect that the particle volume fraction may be no longer uniform in space, but is strongly dependent on the local pressure and velocity fields (see in particular, Behzadmehr et al. [31]). For instance, one may expect that the particle volume fraction could be much higher within the recirculation zone (Fig. 9) than elsewhere in the liquid layer, while it may be lower in the vicinity of the heated surface and other solid walls where high shear stresses are present. Such non-uniform particle distribution in space may, of course, greatly affect both heat diffusion and momentum exchange within the fluid itself, and thus has a direct impact on the local heat transfer as well as on the fluid dynamic behavior. More data and research works are indeed necessary in order to fully understand such rather interesting but somewhat intriguing thermal behaviors of nanofluids.

4. Conclusion

In the present study, we have experimentally investigated the heat transfer behavior of a confined and submerged impinging jet using a nanofluid that is composed of distilled water and 36 nm-average-diameter-Al_2O_3–nanoparticle in suspension. The tests were performed for three different nozzle-to-heated-surface distances, using water and two particular particle volume fractions; the Reynolds and Prandtl numbers are ranging respectively from 3800 to 88 000, and from 5 to 10. Experimental data, obtained for both laminar and turbulent regime, have revealed that depending upon the combination of the nozzle-to-heated surface distance and the particle volume fraction, the use of nanofluids can provide a clear heat transfer enhancement in some cases, while for others combinations, it may even result in an adverse effect on the surface heat transfer coefficient. Within the range of experimental parameters considered, it has been found that highest surface heat transfer coefficients can be achieved using an intermediate nozzle-to-surface distance of 5 mm and the 2.8% particle volume fraction nanofluid. It has also been found that nanofluids with high particle fractions seem not to be appropriate for the heat transfer enhancement purpose under the configuration of a confined and submerged impinging jet. Finally, for the cases with a very small or a large nozzle-to-surface distance, the present experimental data have revealed that the use of nanofluids does not provide any heat transfer enhancement; for some worse cases, a clear decrease of the surface heat transfer coefficient was even found.

Acknowledgement

The authors wish to thank the 'Natural Sciences and Engineering Research Council of Canada' for a financial support to this project. Thanks are also due to the 'Université de Bretagne-Sud' (France) for a financial aid granted to Mr. A. Le Bechec.

References

[1] S.G. Leslie, Cooling options and challenges of high power semiconductors modules, Electronics Cooling 12 (4) (2006) 20–27.
[2] W. Nakayama, Exploring the limits of air cooling, Electronics Cooling 12 (3) (2006) 10–17.
[3] S.U.-S. Choi, Enhancement thermal conductivity of fluids with nanoparticles. Developments and applications of non-Newtonian flows, in: D.A. Siginer, H.P. Wang (Eds.), ASME Publications FED 231/MD 66 (1995) 99–105.
[4] S. Lee, S.U.-S. Choi, Application of metallic nanoparticle suspensions in advanced cooling systems, ASME Publications PVP 342/MD 72 (1996) 227–234.
[5] Nanophase Technologies Corporation, Romeoville, IL, USA, http://www.nanophase.com.
[6] H. Masuda, A. Ebata, K. Teramae, N. Hishinuma, Alteration of thermal conductivity and viscosity of liquid by dispersing ultra-fine particles (dispersion of γ-Al_2O_3, SiO_2 and TiO_2 ultra-fine particles), Netsu Bussei 4 (4) (1993) 227–233.
[7] X. Wang, X. Xu, S.U.S. Choi, Thermal conductivity of nanoparticles-fluid mixture, J. Thermophys. Heat Transfer 13 (4) (1999) 474–480.
[8] C.H. Chon, K.D. Kihm, S.P. Lee, S.U.S. Choi, Empirical correlation finding the role of temperature and particle size for nanofluid (Al_2O_3) thermal conductivity enhancement, Applied Physics Letters 87 (15) (2005) 153107.
[9] S.U.-S. Choi, Z.G. Zhang, W. Yu, F.E. Lockwood, E.A. Grulke, Anamalous thermal conductivity enhancement in nanotube suspensions, Applied Physics Letters 79 (14) (2001) 2252–2254.

[10] J.A. Eastman, S.U.S. Choi, S. Li, W. Yu, L.J. Thompson, Anomalous increase effective thermal conductivities of Ethylene Glycol-based nanofluids containing copper nanoparticles, Applied Physics Letters 78 (6) (2001) 718–720.
[11] G. Roy, C.T. Nguyen, D. Doucet, S. Suiro, T. Maré, Temperature dependent thermal conductivity evaluation of alumina based nanofluids, in: Proc. 13th IHTC, Sydney NSW, Australia, 13–18 August 2006, Begell House, ISBN-1-56700-226-9, 12 p. (CD).
[12] H. Angue Mintsa, G. Roy, C.T. Nguyen, D. Doucet, New temperature dependent thermal conductivity data for water based nanofluids, Int. J. Thermal Sciences 48 (2008) 363–371.
[13] B.C. Pak, Y.I. Cho, Hydrodynamic and heat transfer study of dispersed fluids with submicron metallic oxide particles, Experimental Heat Transfer 11 (2) (1998) 151–170.
[14] Q. Li, Y. Xuan, Convective heat transfer performances of fluids with nanoparticles, in: Proc. 12th Int. Heat Transfer Conference, Grenoble (France), 2002, pp. 483–488.
[15] S.E.B. Maïga, S.J. Palm, C.T. Nguyen, G. Roy, G.N. Galanis, Heat transfer enhancement by using nanofluids in forced convection flows, Int. J. Heat Fluid Flow 26 (4) (2005) 530–546.
[16] G. Roy, C.T. Nguyen, P.-R. Lajoie, Numerical investigation of laminar flow and heat transfer in a radial flow cooling system with the use of nanofluids, Superlattices and Microstructures 35 (3–6) (2004) 497–511.
[17] T. Maré, A.-G. Schmitt, C.T. Nguyen, J. Miriel, G. Roy, Experimental heat transfer and viscosity study of nanofluids: water–γAl_2O_3, in: Proc. 2nd International Conf. Thermal Engineering Theory and Applications, Paper No. 93, January 3–6, 2006, Al Ain, United Arab Emirates.
[18] C.T. Nguyen, G. Roy, P.-R. Lajoie, S.E.B. Maïga, Nanofluids heat transfer performance for cooling of high heat output microprocessor, Paper No. 530-267, IASME Transactions Issue 6 (2), ISSN: 1790-031X, 2005, pp. 994–999.
[19] C.T. Nguyen, G. Roy, C. Gauthier, N. Galanis, Heat transfer enhancement using Al_2O_3 water nanofluid for an electronic liquid cooling system, Applied Thermal Engineering 27 (8–9) (2007) 1501–1506.
[20] C.T. Nguyen, F. Desgranges, G. Roy, N. Galanis, T. Maré, S. Boucher, H.A. Mintsa, Temperature and particle-size dependent viscosity data for water-based nanofluids—hysteresis phenomenon, Int. J. Heat Fluid Flow 28 (6) (2007) 1492–1506.
[21] P. Keblinski, J.A. Eastman, D.G. Cahill, Nanofluids for thermal transport, Materialstoday (June 2005) 36–44.
[22] J.B. Baonga, H. Laouhlia-Gualous, M. Imbert, Experimental study of the hydrodynamic and heat transfer of free liquid jet impinging a flat circular heated disk, Applied Thermal Engineering 26 (2006) 1125–1138.
[23] F. Xu, M.S. Galada, Heat transfer behavior in the impingement zone under circular water jet, Int. J. Heat Mass Transfer 49 (2006) 3785–3799.
[24] T.-W. Lin, M.-C. Wu, L.-K. Liu, C.-J. Fang, Y.-H. Hung, Cooling performance of using a confined slot jet impinging onto heated heat sinks, Trans. ASME J. Electronic Packaging 128 (1) (2006) 82–91.
[25] X. Li, J.L. Gaddis, T. Wang, Multiple flow patterns and heat transfer in confined jet impingement, Int. J. Heat Mass Transfer 26 (2005) 746–754.
[26] T. Akiyama, K. Yamamoto, K.D. Squires, K. Hishida, Simulation and measurement of flow and heat transfer in a two planar impinging jets, Int. J. Heat Fluid Flow 26 (2005) 244–255.
[27] H.G. Lee, H.S. Yoon, M.Y. Ha, A numerical investigation on the fluid flow and heat transfer in the confined impinging slot jet in the low Reynolds number region for different channel heights, Int. J. Heat Mass Transfer 51 (2008) 4055–4068.
[28] V. Katti, S.V. Prabhu, Experimental study and theoretical analysis of local heat transfer distribution between smooth flat surface and impinging air jet from a circular straight pipe nozzle, Int. J. Heat Mass Transfer 51 (2008) 4480–4495.
[29] Y. Xuan, W. Roetzel, Conceptions for heat transfer correlation of nanofluids, Int. J. Heat Mass Transfer 43 (2000) 3701–3707.
[30] K.D. Hagen, Heat Transfer with Applications, Prentice-Hall, 1999.
[31] A. Behzadmehr, M. Saffar-Avval, N. Galanis, Prediction of turbulent forced convection of a nanofluid in a tube with uniform heat flux using a two-phase approach, Int. J. Heat Fluid Flow 28 (2) (2007) 211–219.